Progress In Electromagnetics Research Letters, Vol. 99, 55–63, 2021

Low Divergence Angle OAM Fabry-Perot Antenna with Nonuniform Superstrate

Hui-Fen Huang* **and Qi-Sheng Fan**

Abstract—This paper proposes two low divergence angle orbital angular momentum (OAM) Fabry-Perot (F-P) antennas with nonuniform superstrates. There are two steps to design the proposed two F-P antennas. First, two primary array antennas (a slot array antenna and a patch array antenna) are designed. Both antennas can generate OAM vortex beams with a mode of -1. Second, two F-P resonator cavity antennas are formed by loading a nonuniform partially reflective surfaces (PRS) superstrates above the two primary antennas in order to increase the antenna gain and reduce the divergence angle. The PRS is designed nonuniform for increasing the aperture efficiency. The measured results indicate that the F-P OAM antennas can obviously improve the performance of primary OAM antennas: (1) for the slot array antenna, the divergence angle reduces from 27° to 18°, and the maximum gain increases from 5.2 dBi to 7.5 dBi; (2) for the patch array antenna, the divergence angle decreases from 30° to 18°, and the peak gain increases from 3.4 dBi to 7.2 dBi.

1. INTRODUCTION

In 2007, Thidé et al. firstly proposed that orbital angular momentum can be generated in the radio frequency band [1]. Since then, OAM has received extensive attention in many aspects, such as nanoscopy, astrophysics, and optical communications [2–6]. In theory, there are countless OAM modes, and their different modes are orthogonal and easy to distinguish. Therefore, OAM electromagnetic waves can be transmitted in the same direction without interference, and there can be multiple OAM waves with different modes on the same carrier frequency, which improves channel capacity greatly [7, 8]. OAM waves have been extensively investigated for applications in optical micromanipulation, optical trapping, imaging, free-space optical (FSO) communications, and quantum information processing. To generate OAM-carrying electromagnetic (EM) waves, an azimuthal phase dependence $e^{jl\phi}$ is introduced into the EM waves, where ϕ is the azimuthal angle, and l is an arbitrary integer indicating the topological charge of OAM mode. The methods generating OAM wave mainly include spiral phase plates [9], helicoidal parabolic reflector [10], and uniform circular arrays [11]. It has been experimentally demonstrated that as long as the receiver catches enough power and a suitable phase footprint, OAM yields an increase in capacity, at a given frequency and over a given bandwidth, proportional to the number of transmitted spatial modes [12, 13]. In the meantime, the capacity increases with the enhancement of gain (that is, the decreasing of the OAM beamwidth). For the same size of the receiving antennas, the capacity of the OAM MIMO system is larger than that of the conventional system [14]. However, these apertures quickly become impractical in a communication system at microwave and radio wavelengths due to the expected rapid divergence of beams. More compact apertures such as metasurfaces [15] and patch antenna arrays [16] were introduced to address impracticalities of larger apertures.

Received 19 June 2021, Accepted 26 July 2021, Scheduled 1 August 2021

* Corresponding author: Hui-Fen Huang (huanghf@scut.edu.cn).

The authors are with the School of Electronic and Information Engineering, South China University of Technology, Guangzhou, China.

Nonetheless, some crucial questions are still open, including that the distances of OAM waves are reachable, and the unavoidable divergence of the OAM-carrying beams. In order to increase the gain and decrease the divergence angle, several works have been done. (1) Focusing lens. An additional convex lens is introduced to the OAM beams, and the near-field region can be converged. Hence, the beam divergence is reduced, and then the OAM link range is extended [17]. Two microwave reflectarrays are designed at 12 GHz: one for generation and one for focusing the OAM-carrying beams [18]. (2) Non-diffractive beam. Non-diffractive OAM beam is proposed by a novel 3-dimensional (3-D) printed discrete dielectric lens at 300 GHz [19]. (3) Fabry-Perot Cavity is also used to increase the gain and decrease the divergence angle of the OAM beam. By combining OAM antenna and F-P cavity, the divergence angle is decreased from 41° to 15°, and the gain is enhanced from 4.0 dBi to 12 dBi [20]. A Rotman lens-fed Fabry-Perot resonator antenna with multi-mode beams is proposed in [21]. While loaded with Fabry-Perot Cavity, the antenna achieves directivity enhancement and beam orientation melioration. By using Fabry-Perot Cavity, two circular phased antenna arrays both realize directivity enhancement and divergence angle melioration [22, 23]. A single-layer transmissive metasurface is designed to generate OAM vortex waves [24]. Based on the Fabry-Perot cavity, the proposed antenna achieves gain improvement, homogeneous radiation, and low level posterior lobe radiation. However, currently, the works are still not enough. This paper improves the OAM performance by an improved F-P antenna. The measured results indicate that the improved F-P antenna can greatly decrease the divergence angle and increase the gain. The paper is organized as follows. In Section 2, we introduce the OAM F-P antenna design. The antenna performance is presented in Section 3, and Section 4 is conclusion.

2. OAM F-P ANTENNA DESIGN

The OAM F-P antenna consists of a slot array OAM antenna/patch array OAM antenna (Fig. 1(a)) and a nonuniform PRS superstrate (Fig. 1(b)). The PRS superstrate is located above the array antenna at a height of h_1/h_2 for increasing the gain and decreasing the divergence angle. The array OAM antennas consist of a ground plane and a feed network, which are in each side of an FR4 ($\varepsilon_r = 4.4$, $\tan\delta = 0.02$) substrate with the thickness of $t = 0.8$ mm and lateral size of 84 mm × 84 mm, respectively. The OAM

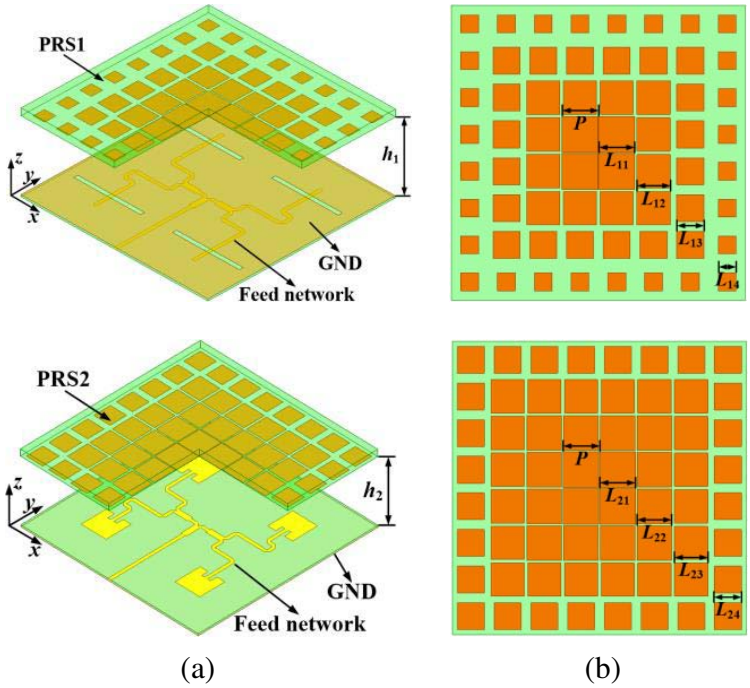

Figure 1. Structure diagrams of (a) slot/patch array antennas. (b) The PRS superstrates.

wave is generated by a sequential feeding network. The PRS superstrate consists of a PRS and an FR4 substrate. The PRS is printed on one side of the FR4 substrate with the overall dimension of 84 mm × 84 mm × 3 mm. The PRS is composed of four kinds of patches with different sizes, which are distributed in four concentric square frames, respectively. The size of the patches is gradually reduced from the center to the edge as shown in Fig. 1(b). The slot array OAM F-P antenna works at 6.41 GHz, and the patch array OAM F-P antenna works at 6.12 GHz. To realize gain enhancement and divergence angle reduction of two array antennas, the PRS is simulated and optimized. All parameters are optimized as follows: $P = 10.5\,\text{mm}$, $L_{11} = 10.3\,\text{mm}$, $L_{12} = 9.5\,\text{mm}$, $L_{13} = 7.7\,\text{mm}$, $L_{14} = 5.1\,\text{mm}$, $h_1 = 30\,\text{mm}$, $L_{21} = 10.3\,\text{mm}$, $L_{22} = 9.9\,\text{mm}$, $L_{23} = 9.5\,\text{mm}$, $L_{24} = 7.7\,\text{mm}$, $h_2 = 29\,\text{mm}$.

The units forming the PRS are a square patch printed on the bottom side of the FR4 substrate as in Fig. 2(a). Fig. 2(b) shows the simulation Floquet ports model of the unit. Fig. 3 shows the reflection coefficients S_{11} of the nonuniform PRS superstrate. The reflection magnitudes of the unit cells decrease from inner to outer regions on the substrate, which indicate that the PRS units own negative transverse-reflection magnitude gradient properties to achieve the equal amplitude and cophasal distributions respectively for its aperture electromagnetic field, and therefore improve its aperture efficiency [25].

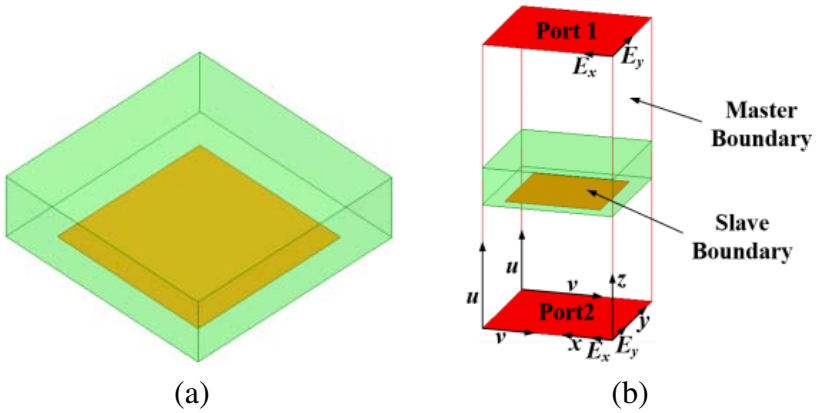

Figure 2. (a) Structure of the unit. (b) Simulation model of the unit.

To achieve a maximum gain, the resonance condition should be satisfied as follows [21]:

$$\varphi_{\text{PRS}} + \varphi_G + 2N\pi = \frac{4\pi f\left(h + t\sqrt{\varepsilon_r}\right)\cos\theta}{c}, \quad N = 0, 1, 2... \tag{1}$$

where h is the height of the cavity, f the operation frequency, t the thickness of the substrate, ε_r the relative dielectric constant, θ the angle between normal direction of the floor and electromagnetic waves direction, and φ_{PRS} and φ_G are the reflection coefficient phases of the PRS and the ground, respectively.

In general, the maximum mode of an OAM antenna is determined by the number of elements in the circular array. The maximum mode of an OAM antenna with N antenna elements is $|l| < N/2$. To generate an OAM mode $l = -1$ with four antenna elements, the antenna elements should be divided into four uniform amplitudes with a sequential $2\pi l/N = -\pi/2$ phase difference for the consecutive elements. That is, the phase increases by 90° counterclockwise as shown in Fig. 4.

3. ANTENNA PERFORMANCE

To verify the effectiveness of the F-P antenna for increasing the gain and decreasing the divergence angle, numerical simulations are performed for the slot array/patch array antenna with and without the nonuniform PRS superstrate. The simulation software Ansoft HFSS is used to simulate the radiation performance of the antennas.

The simulated near-field phase distribution and far-field 3-D radiation patterns of the primary OAM antennas (the slot array antenna/patch array antenna) and the OAM F-P antenna with $l = -1$

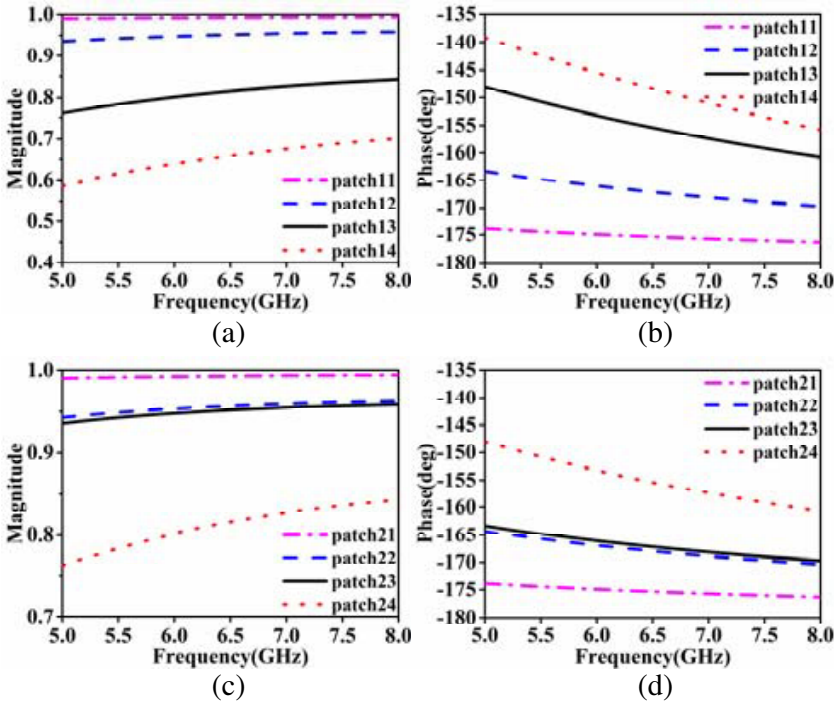

Figure 3. Reflection coefficients (S_{11}) of patch units. For PRS1: (a) Magnitude. (b) Phase. For PRS2: (c) Magnitude. (d) Phase.

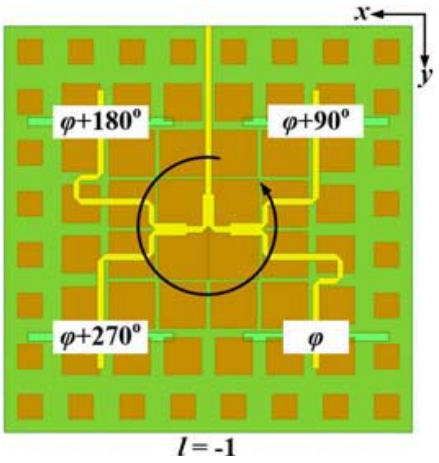

Figure 4. Phase distribution diagram of antenna elements with OAM mode $l = -l$.

at ($\theta = 0°$, $\phi = 0°$) are presented in Fig. 5. The zero-intensity area caused by the phase singularity of the OAM beam clearly exists in the center of the plane as a "black hole," and the helical phase pattern proves the phase change of the OAM beams with mode $l = -1$. Compared with the primary OAM antenna, the electromagnetic waves radiated by the F-P OAM antennas are more uniform and stronger in the annular region, and the divergence angles are obviously decreased. The nonuniform PRS superstrate increases the maximum gain from 3.9 dBi to 7.9 dBi for the slot array antenna, and the maximum gain is enhanced from 3.3 dBi to 7.1 dBi for the patch array antenna. The aperture efficiencies are 15.2% and 13.9% for the slot array antenna and the patch array antenna, respectively.

In order to validate the design, two OAM antenna arrays are fabricated and measured. The prototypes and measurement circumstances of the two F-P OAM antennas are shown in Fig. 6. The

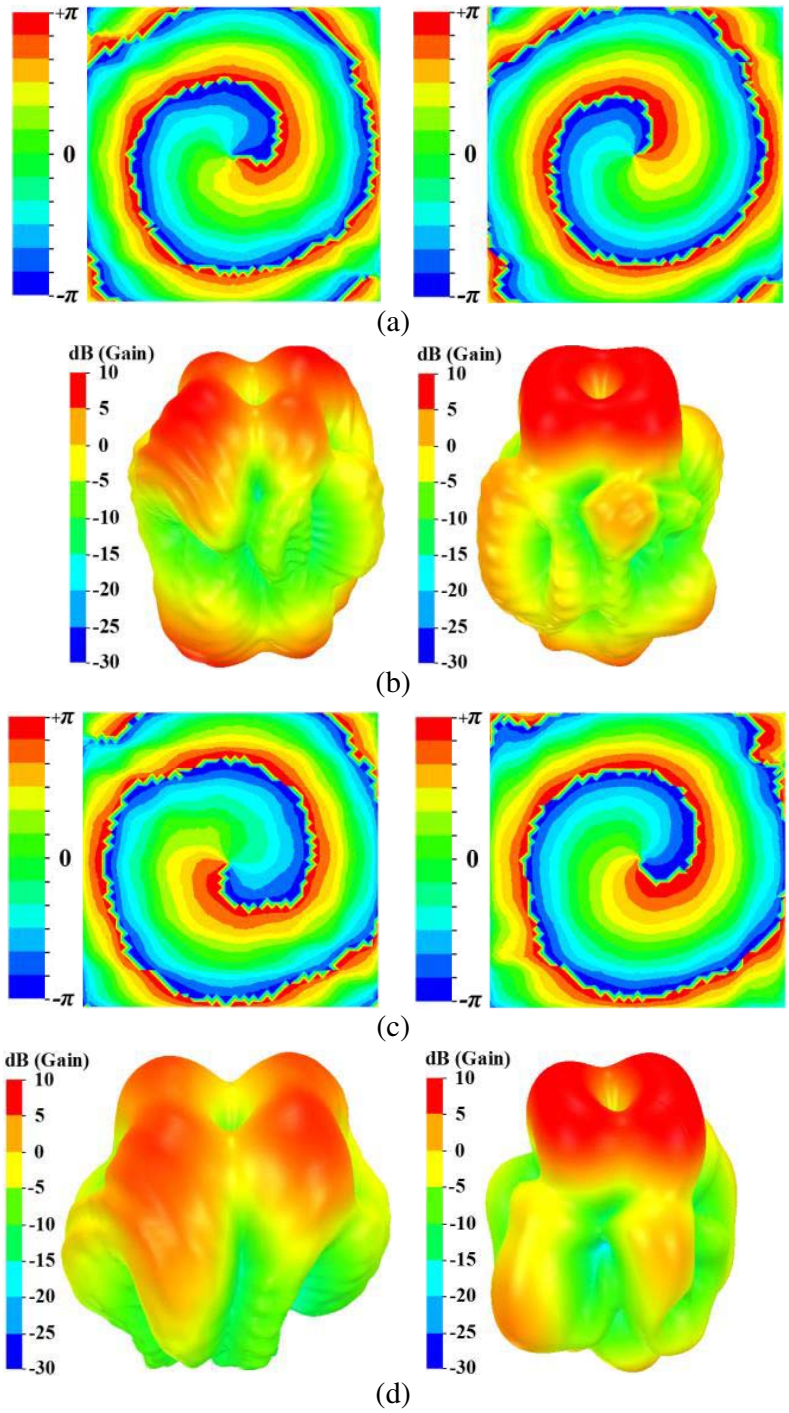

Figure 5. (a), (b) Phase distribution and 3D pattern of the slot array antenna and its F-P OAM antenna at 6.41 GHz. (c), (d) Phase distribution and 3D pattern of the patch array antenna and its F-P OAM antenna at 6.12 GHz.

nonuniform PRS superstrate and the array antenna are supported by four nylon spacers. Fig. 7 shows the simulated and measured results of the reflection coefficients S_{11} of two OAM antennas with/without superstrates. For the slot array antenna, the measured impedance bandwidths ($S_{11} < -10$ dB) with/without superstrate are 30.3% (5.76–7.82 GHz) and 29.9% (5.7–7.7 GHz), respectively. For the

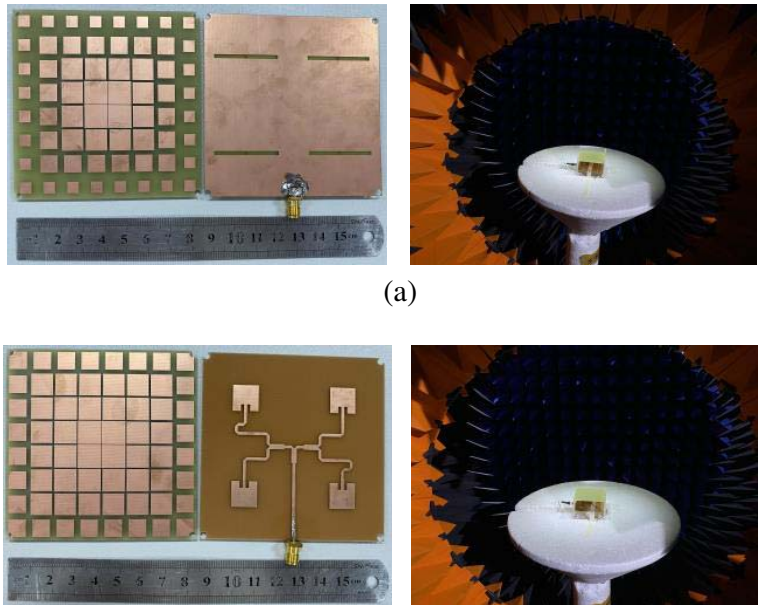

Figure 6. The prototypes and measurement circumstances of two OAM antennas. (a) The slot array antenna loaded with PRS1. (b) The patch array antenna loaded with PRS2.

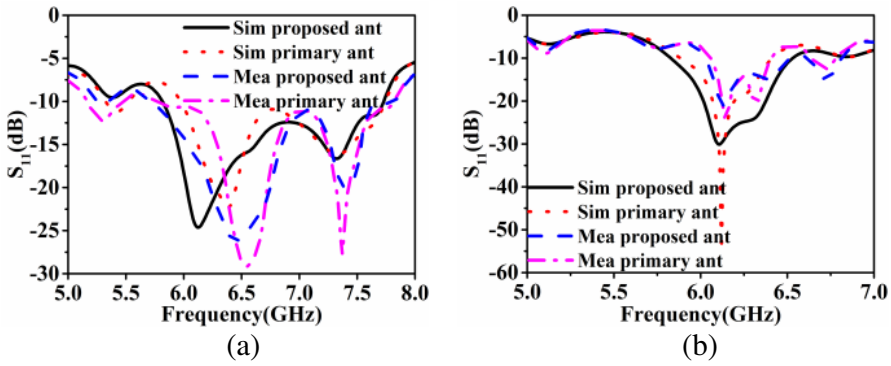

Figure 7. Simulated and measured S_{11}. (a) The slot array antenna and OAM antenna. (b) The patch array antenna and OAM antenna.

patch array antenna, the measured impedance bandwidths ($S_{11} < -10$ dB) with/without superstrate are 5.6% (6.06–6.41 GHz) and 7.8% (6.03–6.52 GHz), respectively. Fig. 8 shows the radiation patterns of the slot array antenna with/without PRS superstrate at 6.41 GHz with mode -1. It can be found that the pattern has a hollow in the axial direction. The measured divergence angles for slot array antenna with/without PRS superstrate are 18° and 27°, respectively, and the F-P antenna decreases the divergence angle by 9°. The measured maximum gain with PRS superstrate is 7.5 dBi, and gain is increased by 2.3 dBi compared with the primary antenna. The measured aperture efficiency is 13.9%. For the patch array antenna, the measured divergence angles for with/without superstrate are 18° and 30°, respectively. The peak gain of the OAM F-P antenna is 7.2 dBi, and the superstrate increases the gain 3.8 dBi compared with the primary patch array. It can be seen that the nonuniform PRS superstrates can increase the gains and decrease the divergence angles of the primary antennas greatly. The measured aperture efficiency is 14.2%. In addition, the simulated and measured results agree well as shown in Fig. 8.

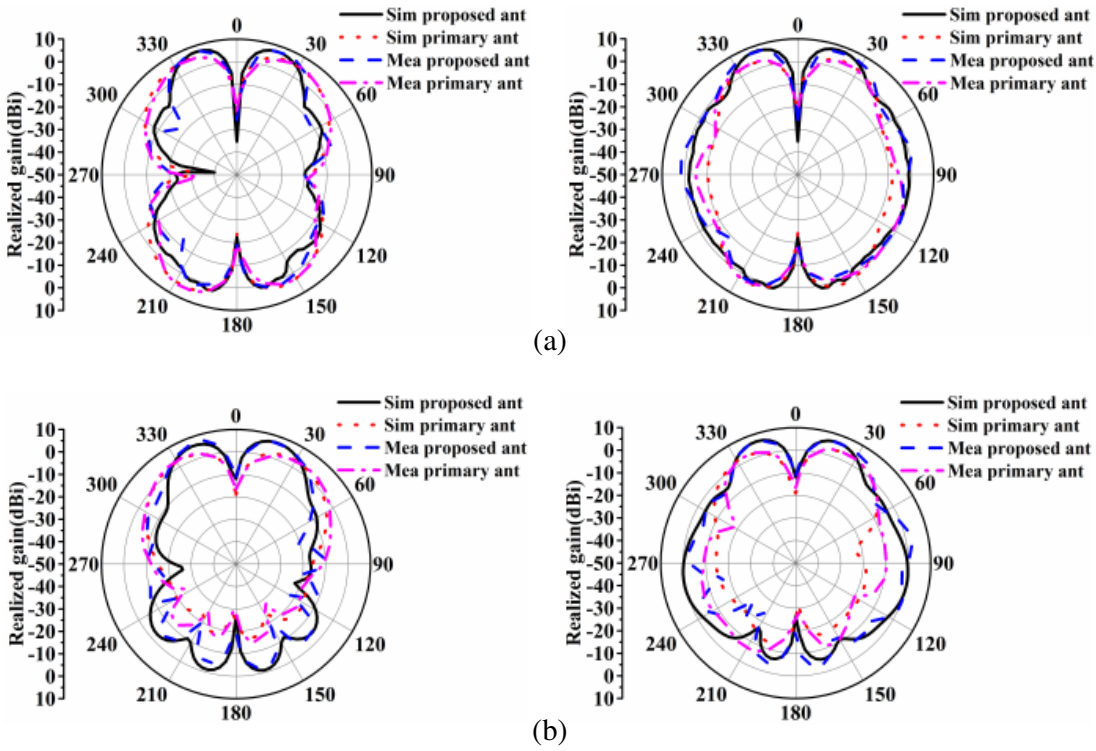

Figure 8. The radiation pattern of the slot array antenna loaded with PRS1 at 6.41 GHz. (b) The radiation pattern of the patch array antenna loaded with PRS2 at 6.12 GHz.

4. CONCLUSION

This paper proposes two F-P OAM antenna arrays with nonuniform PRS superstrate. Compared with primary antennas, the nonuniform PRS superstrate can greatly increase the gain and decrease the divergence angle of the OAM waves. Compared with the primary antenna: (1) For the slot array antenna, the F-P antenna decreases the divergence angle by 9° and increases the gain by 2.3 dBi. (2) For the patch array antenna, the nonuniform PRS superstrate decreases the divergence angle by 12° and increases the gain by 3.8 dBi.

ACKNOWLEDGMENT

This work was supported by the Key Project of Natural Science Foundation of Guangdong Province of China under Grant 2018B030311013, the National Natural Science Foundation of China under Grant 61071056.

REFERENCES

1. Thidé, B., et al., "Utilization of photon orbital angular momentum in the low-frequency radio domain," *Phys. Rev. Lett.*, Vol. 99, No. 8, Art. no. 087701, Aug. 2007.
2. Hell, S. W., "Toward fluorescence nanoscopy," *Nature Biotechnol.*, Vol. 21, 1347–1355, Oct. 2003.
3. Harwit, M., "Photon orbital angular momentum in astrophysics," *Astrophys. J.*, Vol. 597, 1266–1270, Nov. 2003.
4. Leach, J., B. Jack, J. Romero, A. K. Jha, A. M. Yao, S. Franke-Arnold, D. G. Ireland, R. W. Boyd, S. M. Barnett, and M. J. Padgett, "Quantum correlations in optical angle-orbital angular momentum variables," *Science*, Vol. 329, 662–665, Aug. 2010.

5. Paterson, C., "Atmospheric turbulence and orbital angular momentum of single photons for optical communication," *Phys. Rev. Lett.*, Vol. 94, Art. no. 153901, Apr. 2005.
6. Shapiro, J., S. Guha, and B. Erkmen, "Ultimate channel capacity of free-space optical communications," *J. Opt. Netw.*, Vol. 4, No. 8, 501–516, 2005.
7. Wang, J., J.-Y. Yang, I. M. Fazal, N. Ahmed, Y. Yan, H. Huang, Y. Ren, Y. Yue, S. Dolinar, M. Tur, and A. E. Willner, "Terabit free-space data transmission employing orbital angular momentum multiplexing," *Nature Photon.*, Vol. 6, 488–496, Jun. 2012.
8. Bai, X., X. Liang, R. Jin, and J. Geng, "Generation of OAM radio waves with three polarizations using circular horn antenna array," *Proc. 9th Eur. Conf. Antennas Propag. (EuCAP)*, 1–4, Apr. 2015.
9. Hui, X., et al., "Ultralow reflectivity spiral phase plate for generation of millimeter-wave OAM beam," *IEEE Antennas Wireless Propag. Lett.*, Vol. 14, 966–969, 2015.
10. Byun, W.-J., Y.-S. Lee, B. S. Kim, K. S. Kim, M. S. Kang, and Y. H. Cho, "Simple generation of orbital angular momentum modes with azimuthally deformed cassegrain subreflector," *Electron. Lett.*, Vol. 51, No. 19, 1480–1482, 2015.
11. Bai, Q., A. Tennant, and B. Allen, "Experimental circular phased arrayfor generating OAM radio beams," *Electron. Lett.*, Vol. 50, No. 20, 1414–1415, Sep. 2014.
12. Tamburini, F., E. Mari, A. Sponselli, B. Thidé, A. Bianchini, and F. Romanato, "Encoding many channels on the same frequency through radio vorticity: First experimental test," *New J. Phys.*, Vol. 14, No. 3, 033001, 2012.
13. Yan, Y., et al., "High-capacity millimetre-wave communications with orbital angular momentum multiplexing," *Nat. Commun.*, Vol. 5, 4876, 2014.
14. Xue, W., X. Chen, X. Liu, X. Meng, A. Zhang, and W. E. I. Sha, "A revisit of orbital angular momentum multiplexing in multipath environment," *Journal of Communications and Information Networks*, Vol. 5, No. 4, 438–446, Dec. 2020.
15. Huang, H.-F. and S.-N. Li, "Single-layer dual-frequency unit for multifunction OAM reflectarray applications at the microwave range," *Opt. Lett.*, Vol. 45, No. 18, 5165–5168, 2020.
16. Li, W., L. Zhang, S. Yang, K. Zhuo, L. Ye, and Q. H. Liu, "A reconfigurable second-order OAM patch antenna with simple structure," *IEEE Antennas Wireless Propag. Lett.*, Vol. 19, No. 9, 1531–1535, Sep. 2020.
17. Allen, B., et al., "Reduction of orbital angular momentum radio beam divergence using a 3D printed planar graded index lenses," *Proc. 12th Eur. Conf. Antennas Propag. (EuCAP)*, 1–3, London, U.K., 2018.
18. Li, F., et al., "Generation and focusing of orbital angular momentum based on polarized reflectarray at microwave frequency," *IEEE Transactions on Microwave Theory and Techniques*, Vol. 69, No. 3, 1829–1837, Mar. 2021.
19. Wu, G.-B., K. F. Chan, and C. H. Chan, "3-D printed terahertz lens to generate higher-order Bessel beams carrying OAM," *IEEE Trans. Antennas Propag.*, Vol. 69, No. 6, 3399–3408, Jun. 2021.
20. Yao, Y., X. Liang, R. Jin, and J. Geng, "Analysis of focusing orbital angular momentum wave using Fabry-Perot cavity," *Journal of Communications and Information Networks*, Vol. 4, No. 3, 9–17, Sept. 2019.
21. Bai, X., "Rotman lens-fed Fabry-Perot resonator antennas for generating converged multi-mode OAM beams," *IEEE Access*, Vol. 7, 105768–105775, 2019.
22. Wei, W. L., K. Mahdjoubi, C. Brousseau, O. Emile, and A. Sharaiha, "Enhancement of directivity of an OAM antenna by using Fabry-Perot cavity," *2016 10th European Conference on Antennas and Propagation (EuCAP)*, 1–4, Davos, 2016.
23. Bai, X., Y. Sun, P. Hu, J. Chen, W. Yan, X. Liang, C. He, J. Geng, and R. Jin, "Improvement on the multi-mode beams divergence of OAM array by using Fabry-Perot cavity," *Proc. IEEE Int. Symp. Antennas Propag. USNC/URSI Nat. Radio Sci. Meeting*, 2193–2194, IEEE, San Diego, CA, USA, Jul. 2017.

24. Ma, L., C. Chen, L. Zhou, S. Jiang, and H. Zhang, "Single-layer transmissive metasurface for generating OAM vortex wave with homogeneous radiation based on the principle of Fabry-Perot cavity," *Appl. Phys. Lett.*, Vol. 114, No. 8, Art. no. 081603, 2019.
25. Lian, R., Z. Tang, and Y. Yin, "Design of a broadband polarization reconfigurable Fabry-Perot resonator antenna," *IEEE Antennas Wireless. Propag. Lett.*, Vol. 17, No. 1, 122–125, Jan. 2018.